SPECIAL TOPIC — Non-equilibrium phenomena in soft matters

Mechanical properties of jammed packings of frictionless spheres under an applied shear stress*

Liu Hao(刘 浩), Tong Hua(童 华), and Xu Ning(徐 宁)†

Key Laboratory of Soft Matter Chemistry of Chinese Academy of Sciences, Hefei National Laboratory for Physical Sciences at the Microscale, and Department of Physics, University of Science and Technology of China, Hefei 230026, China

(Received 16 June 2014; published online 17 September 2014)

By minimizing a thermodynamic-like potential, we unbiasedly sample the potential energy landscape of soft and frictionless spheres under a constant shear stress. We obtain zero-temperature jammed states under desired shear stresses and investigate their mechanical properties as a function of the shear stress. As a comparison, we also obtain the jammed states from the quasistatic-shear sampling in which the shear stress is not well-controlled. Although the yield stresses determined by both samplings show the same power-law scaling with the compression from the jamming transition point J at zero temperature and shear stress, for finite size systems the quasistatic-shear sampling leads to a lower yield stress and a higher critical volume fraction at point J. The shear modulus of the jammed solids decreases with increasing shear stress. However, the shear modulus does not decay to zero at yielding. This discontinuous change of the shear modulus implies the discontinuous nature of the unjamming transition under nonzero shear stress, which is further verified by the observation of a discontinuous jump in the pressure from the jammed solids to the shear flows. The pressure jump decreases upon decompression and approaches zero at the critical-like point J, in analogy with the well-known phase transitions under an external field. The analysis of the force networks in the jammed solids reveals that the force distribution is more sensitive to the increase of the shear stress near point J. The force network anisotropy increases with increasing shear stress. The weak particle contacts near the average force and under large shear stresses it exhibit an asymmetric angle distribution.

Keywords: jamming, shear, phase transition, force network

PACS: 61.43.–j **DOI:** 10.1088/1674-1056/23/11/116105

1. Introduction

Athermal particulate systems, such as foams and granular materials, undergo a jamming transition at point J when the packing density increases to a critical value.[1–5] This jamming transition is signified by the sudden formation of rigidity to resist shear and compression, which resembles the typical noncrystalline liquid–solid transitions, such as the glass transition and the yielding of amorphous solids under shear. Compared to the glass transition and the yielding, the jamming transition at point J seems simpler due to the absence of dynamics. People believe that there are common underlying mechanisms for these different transitions, although they are driven by different parameters, such as, volume fraction (density) ϕ for the jamming transition and the glass transition, temperature T for the glass transition, and shear stress σ for the yielding. This has inspired the idea of unifying these different transitions in the same framework of the jamming phase diagram.[1,2,6]

The standing of point J in the jamming phase diagram is significant. It is the upper limit of the glass transition of hard spheres and the ending point of the yielding of jammed packings of repulsive particles in the zero shear stress limit. Therefore, studying the jamming transition at point J and the properties of the jammed solids at $T = 0$ will definitely shed light on our understanding of noncrystalline liquid–solid transitions in general. As a unique transition, the jamming transition at point J exhibits unusual critical behaviors, which have received extensive concerns in the past decade.[7–24] Most of the previous studies have been focused on marginally jammed solids near point J at $T = 0$ and $\sigma = 0$. Only recently has the influence of the applied shear stress on the jamming attracted some attention. For instance, it has been shown that the critical volume fraction ϕ_c at point J moves to a higher value when the jamming threshold is probed in quasistatically sheared systems.[8,25]

In addition to the jamming transition, how the jammed solids respond to the applied shear stress is of great importance for understanding the mechanical failure of materials, especially for granular materials. As is well known, in granular materials the particle contacts constitute a force network.[26] Due to the structural disorder, the contact forces are spatially heterogeneous and show a wide distribution.[27–30] It has been proposed that the force network can be separated into two subnetworks, a strong one with contact forces higher than the average and a weak one otherwise. When being sheared,

*Project supported by the National Natural Science Foundation of China (Grant No. 21325418), the National Basic Research Program of China (Grant No. 2012CB821500), the Chinese Academy of Sciences 100-Talent Program (Grant No. 2030020004), and the Fundamental Research Funds for the Central Universities, China (Grant No. 2340000034).

†Corresponding author. E-mail: ningxu@ustc.edu.cn

© 2014 Chinese Physical Society and IOP Publishing Ltd

these two subnetworks exhibit both geometric and mechanical anisotropies which are interestingly complementary.[31–33] However, a concrete picture of the evolution of the force network anisotropy with the applied shear stress is still lacking.

The major difficulty to study jamming under an applied shear stress is the lack of an efficient method to explore the potential energy landscape and find the local potential energy minima under the constraint of a constant shear stress. In most of the previous simulations, people applied a quasistatic shear by successively applying a step shear strain followed by the energy minimization.[25,34–38] In such an approach, the shear stress is not a well-controlled quantity. In reality, shearing is mostly triggered by the shear force instead of the shear strain. Recently, we reported an efficient method to find the local potential energy minima under a constant shear stress by minimizing a thermodynamic-like potential.[7] This new method enables us to generate jammed solids under a desired shear stress and thus study how their properties vary with the shear stress by unbiasedly sampling the potential energy landscape.

As briefly discussed in Ref. [7], compared to the unbiased sampling of our new method, the quasistatic shear tends to explore the low-energy regions of the potential energy landscape. It is interesting then to know whether and how these two approaches differ from each other in the description of the jamming under an applied shear stress. We use CS and QS to denote the constant shear stress sampling and the quasistatic-shear sampling. In this paper, we are mainly concerned with the mechanical properties of the jammed solids under an applied shear stress, including the yield stress, the shear modulus, and the force networks, with comparisons between the CS and the QS samplings. The structure of this paper is as follows. In Section 2, we introduce the details of our simulation model and the two samplings. In Section 3, we compare the QS sampling with the CS sampling in the measurement of the critical scaling of the yield stress. In Section 4, we discuss the discontinuous nature of the unjamming transition at $\sigma > 0$ by showing the discontinuous change of the shear modulus and pressure. In Section 5, we focus on the shear stress dependence of the force distribution and the force network anisotropy. We conclude our work in Section 6.

2. Simulation model and methods

Our systems are three-dimensional boxes with side length L in all directions, which contain N frictionless spheres. We apply the Lees–Edwards boundary condition in the z direction and the periodic boundary conditions in both x and y directions to mimic shearing.[39] The shear force is applied in the x direction, and the shear gradient is along the z direction. To avoid crystallization, we use $N/2$ large and $N/2$ small particles with equal mass m, and the diameter ratio is 1.4. The interaction potential between particles i and j is harmonic

$$U_{ij} = \frac{\varepsilon}{2}\left(1 - \frac{r_{ij}}{d_{ij}}\right)^2 \Theta\left(1 - \frac{r_{ij}}{d_{ij}}\right), \tag{1}$$

where r_{ij} is their separation, d_{ij} is the sum of their radii, and $\Theta(x)$ is the Heaviside function. We set the units of mass, energy, and length to be m, ε, and small particle diameter d_s, respectively.

To perform the QS sampling, we start with 1000 distinct jammed states generated by minimizing the total potential energy $U = U(\boldsymbol{r}_1, \boldsymbol{r}_2, \ldots, \boldsymbol{r}_N, \gamma = 0)$ of random states using the fast inertial relaxation engine (FIRE) minimization method.[40] A step shear strain $\Delta\gamma = 10^{-4}$ is then applied to these states, followed by the FIRE minimization of $U(\boldsymbol{r}_1, \boldsymbol{r}_2, \ldots, \boldsymbol{r}_N, \gamma = \Delta\gamma)$. The same procedure is repeated until the system is sheared up to a unit strain $\gamma = 1$. The whole process therefore mimics the shear flow in the zero shear rate limit. For each initial state, we obtain 10000 states under different shear stresses. As shown in the inset of Fig. 1(a), every point on the σ–γ curve represents a state sampled by the QS sampling. Apparently, in the QS sampling, the states sampled are historically dependent and the shear stress cannot be controlled. To investigate the shear stress dependence of the states obtained by the QS sampling, we bin the shear stress using an interval Δ and average the states with the shear stress lying in $(\sigma - \Delta/2, \sigma + \Delta/2)$.

In order to obtain the jammed states under desired shear stress σ, we start with random states and minimize the thermodynamic-like potential[7]

$$H(\boldsymbol{r}_1, \boldsymbol{r}_2, \ldots, \boldsymbol{r}_N, \gamma) = U(\boldsymbol{r}_1, \boldsymbol{r}_2, ..., \boldsymbol{r}_N, \gamma) - \sigma\gamma L^3 \tag{2}$$

using the FIRE minimization method. Equation (2) is the Legendre transformation of the potential energy $U(\boldsymbol{r}_1, \boldsymbol{r}_2, \ldots, \boldsymbol{r}_N, \gamma)$ to change the control parameter from the shear strain γ (QS sampling) to the shear stress σ (CS sampling). By minimizing H, the local potential energy minima with a shear stress σ can be obtained, so we are able to realize the CS sampling. In contrast to the QS sampling, in which the energy minimization is performed under a fixed shear strain, the shear strain during the minimization of the CS sampling is changing. The shear strain is initially set to be zero, which increases during the minimization until a jammed state with the shear stress σ is found. Since the initial states are randomly selected, this CS sampling unbiasedly samples the potential energy landscape.

3. Critical scaling of the yield stress

In Ref. [7], we apply the CS sampling to measure the probability of finding the jammed states under a constant shear stress. At $\phi > \phi_c$, when the shear stress is small, the probability is one, while it decays to zero when the shear stress is large.

We define the yield stress as the shear stress at which the probability is 0.5. It is thus the critical shear stress in the potential energy landscape perspective, above which it is hard to find the jammed states able to sustain the applied shear stress. The yield stress of jammed systems with harmonic repulsion from the CS sampling is linearly scaled with $\phi - \phi_c$.

In the literature, the yield stress is usually defined in the shear flow perspective; that is, it is the average shear stress in the zero shear rate limit. It can be obtained by fitting the flow curve $\sigma(\dot{\gamma})$ with empirical expressions,[41] such as, the Herschel–Buckley relation $\sigma = \sigma_y + A\dot{\gamma}^{\alpha}$, where $\dot{\gamma}$ is the shear rate, $\sigma_y = \sigma(0)$ is the yield stress, and A and α are the fitting parameters. This yield stress can also be directly measured from the QS sampling. Figure 1(a) shows $\sigma(\gamma)$ averaged over 1000 independent QS runs. A single QS flow consists of lots of segments of elastic deformations (linear increase of σ with γ) followed by a plastic event (sudden stress drop), as shown in the inset of Fig. 1(a). On average, the shear stress exhibits an initial increase with γ before reaching a plateau. The yield stress is thus defined as the plateau value of the shear stress.

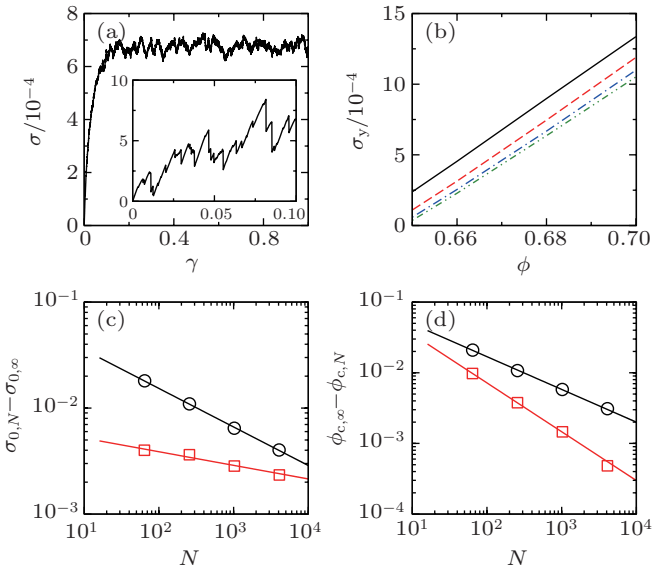


Fig. 1. (a) Shear stress σ versus shear strain γ for jammed solids consisting of $N = 1024$ particles at $\phi = 0.68$ averaged over 1000 independent runs of quasistatic shear. The inset shows an example of a single QS run. (b) Volume fraction ϕ dependence of yield stress σ_y for systems with $N = 64$, 256, 1024, and 4096 from the top to the bottom. (c) and (d) System size dependences of fitting parameters $\sigma_{0,N}$ and $\phi_{c,N}$ for the CS (circles) and the QS (squares) samplings. The lines are the fits to the data using the formula discussed in the text.

Figure 1(b) shows the volume fraction and the system size dependences of the yield stress measured from the QS sampling. The yield stress is linear in the volume fraction well above point J, $\sigma_y = \sigma_{0,N}(\phi - \phi_{c,N})$, where $\sigma_{0,N}$ and $\phi_{c,N}$ are the fitting parameters, $\phi_{c,N}$ is also the average volume fraction of point J for finite systems with N particles. In Figs. 1(c) and 1(d), we compare the system size dependences of $\sigma_{0,N}$ and $\phi_{c,N}$ between the QS and the CS samplings. For both samplings, we fit $\sigma_{0,N}$ and $\phi_{c,N}$ into $\sigma_{0,N} = \sigma_{0,\infty} + a_\sigma N^{-b_\sigma}$ and $\phi_{c,N} = \phi_{c,\infty} - a_\phi N^{-b_\phi}$ with the fitting parameters shown in Table 1.

Table 1. Fitting parameters of the power-law scaling of $\phi_{c,\infty} - \phi_{c,N}$ and $\sigma_{0,N} - \sigma_{0,\infty}$ shown in Figs. 1(c) and 1(d).

	$\phi_{c,\infty}$	a_ϕ	b_ϕ	$\sigma_{0,\infty}$	a_σ	b_σ
CS	0.649	0.137	0.457	0.018	0.082	0.363
QS	0.649	0.173	0.691	0.018	0.007	0.128

For the finite size systems studied here, the yield stress from the CS sampling is larger than that from the QS sampling. The gap between the two yield stresses decreases when the system size increases. The yield stress from the CS sampling is by definition the maximum stress under which the jammed states can survive, while the yield stress from the QS sampling is the average stress of the jammed states under shear. For the finite size systems, the yield stress from the CS sampling measures the upper limit of the stress fluctuations, as shown in the inset of Fig. 1(a), which explains the existence of the gap between the two yield stresses. When the system size increases, the stress fluctuations decay, which leads to the decrease of the gap. It is thus expected that in the thermodynamic limit the two yield stresses are equal because the stress fluctuations vanish, as also claimed in Ref. [42].

Figure 1(d) indicates that $\phi_{c,N}$ estimated from the QS sampling is larger than that from the CS sampling. In Ref. [7], we attribute it to the fact that the QS sampling tends to explore the low-energy states, which is a demonstration of the historic dependence of the QS sampling. For the finite size systems, the volume fraction of the jamming transition at point J is not well-defined but is broadened to a distribution with a width w due to the finite size effect.[2] The w decreases when increasing the system size and vanishes in the thermodynamic limit.[2] In the distribution, the probability of finding the jammed states $P_J(\phi)$ increases from 0 to 1 when the volume fraction ϕ increases. For unbiased samplings, like the CS sampling, $P(\phi) = dP_J(\phi)/d\phi$ is approximately Guassian-like, and $\phi_{c,N}$ is the volume fraction at which $P(\phi)$ has the maximum and the probability of finding the jammed states is approximately 0.5. However, because the QS sampling tends to explore the low-energy states, it is more likely to find the unjammed states, so the probability of finding the jammed states being 0.5 is pushed to a higher $\phi_{c,N}$ than that in the CS sampling. In the thermodynamic limit, $\phi_{c,\infty}$ should be well-defined and independent of ways of sampling, we thus expect that $\phi_{c,\infty}$ for both samplings are identical. As shown in Fig. 1, we use the same $\phi_{c,\infty}$ and $\sigma_{0,\infty}$ for both the CS and the QS samplings, and can indeed fit the data well.

4. Discontinuous unjamming transition at $\sigma > 0$

When the applied shear stress increases to the yield stress, the marginally jammed solids are expected to be softened and

unjam to shear flows. As discussed above, in the thermodynamic limit, the yield stress vanishes at the well-defined point J at $\phi_{c,\infty}$. The criticality of point J has been widely discussed,[7–24] although the nature of the jamming transition at point J has not come to a conclusion. If we assume that point J is critical, then the jamming phase diagram in the σ–ϕ plane at $T = 0$ reminisces the typical phase transitions like the paramagnetic–ferromagnetic and the superconducting transitions under an external magnetic field, in which the transition is critical in the absence of the magnetic field while discontinuous when the field is nonzero. Is the unjamming transition at $\sigma > 0$ also discontinuous?

In Fig. 2(a), we compare the shear moduli G of the jammed solids obtained from the CS and the QS samplings under different shear stresses up to the yield stress. For both samplings, the shear modulus decreases and the solid is softened when the shear stress increases. Under the same shear stress, the shear modulus from the QS sampling is, in general, a little bit smaller than that from the CS sampling. This is consistent with the fact that the QS sampling moves $\phi_{c,N}$ to a higher value compared with the CS sampling. Because the shear modulus is proportional to $(\phi - \phi_{c,N})^{1/2}$,[2] at the same volume fraction, the jammed solids from the QS sampling are closer to point J and thus have a smaller G. Figure 2(a) also shows that for both samplings, the shear modulus does not go to zero at yielding. When the applied shear stress is higher than the yield stress, the system flows forever with $G = 0$, so there is a discontinuous change of the shear modulus from $G > 0$ to $G = 0$ at yielding when the yield stress $\sigma_y > 0$. This provides evidence that the unjamming transition at $\sigma > 0$ is discontinuous.

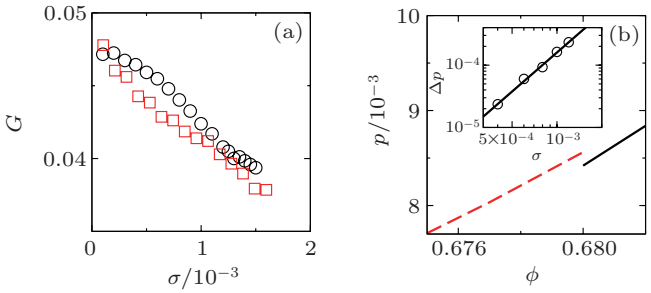


Fig. 2. (a) Shear stress σ dependence of shear modulus G measured from the CS (circles) and the QS (squares) samplings. The systems are jammed solids consisting of $N = 1024$ particles at $\phi = 0.70$. (b) Volume fraction dependence of the pressure measured at $\sigma = 10^{-3}$ for $N = 1024$ systems. Solid and dashed curves are measured for the jammed solids and the unjammed shear flows, respectively. The inset shows the shear stress dependence of the pressure gap between unjammed and jammed states, Δp, at yielding for $N = 1024$ systems. The line shows the relation $\Delta p \sim \sigma^2$.

Figure 2(b) shows another evidence of the discontinuous unjamming transition at $\sigma > 0$. Under a fixed shear stress σ, when the volume fraction increases, the systems undergo the jamming transition from unjammed (steadily flowing) states to jammed solids at the crossover volume fraction ϕ_y determined by $\sigma = \sigma_y(\phi_y)$. When $\phi < \phi_y$, the CS sampling can also generate the unjammed states under the constant shear stress σ. We can then compare the pressure of the jammed solids with that of the unjammed flowing states at ϕ_y.

As shown in Fig. 2(b), there is a small discontinuity in the pressure around ϕ_y. The pressure of the unjammed states is higher than that of the jammed solids at ϕ_y. Note that here we only take into account the excess part of the pressure arising from the particle interactions and exclude the ideal gas contribution because our CS minimization is not a real dynamical process and does not capture the particle velocities. For the unjammed states, if the shear rate is zero at the yield stress, the ideal gas term of the pressure is negligible. However, the previous studies have shown that, for viscoelastic shear flows driven by a constant shear stress, the critical shear rate at the yield stress defined as the minimum shear stress below which the systems eventually cease flowing may not vanish for finite size systems.[42,43] If there will be an ideal gas contribution to the pressure of the unjammed states at the yield stress, this leads to an even larger pressure gap than that shown in Fig. 2(b). In any case, the presence of the pressure gap, although small compared to the pressure itself, also implies that the unjamming transition at $\sigma > 0$ is discontinuous.

The inset of Fig. 2(b) shows the pressure gap, $\Delta p = p_u - p_j$, at yielding as a function of the shear stress for $N = 1024$ systems, where p_u and p_j are the pressures of the unjammed and the jammed states, respectively. Our data suggest a possible relation $\Delta p \sim \sigma^2 \sim p^2 \sim G^4$, which indicates the trend of a decreasing gap with decreasing shear stress. This is consistent with the criticality of point J in the thermodynamic limit and in analog with those conventional phase transitions under an external magnetic field. Our study here presents some evidence to suggest the discontinuous nature of the yielding (unjamming transition at $\sigma > 0$) of the jammed states as a possible phase transition. However, further investigations are required to verify our suggestion with the key to find the correct order parameter to characterize the transition.

5. Anisotropic force networks in jammed solids at $\sigma > 0$

For jammed packings of grains, such as, sand piles, the contact forces between the grains form a spatially heterogeneous force network. When subject to a load, the force network becomes anisotropic and directional, forming percolating force chains to support the load.[32] Jammed packings of spheres near point J are the typical model systems to study the force networks in granular materials. It has been shown

that the distribution of the contact force $P(F)$ in jammed packings of frictionless spheres near point J in general decreases when increasing the force with an exponential decay at large F.[27–30,33] For systems with harmonic repulsion, a maximum in $P(F)$ at small F emerges when the jamming transition is approached from the unjammed side.[27] By applying the CS sampling to generate jammed solids under desired shear stresses, we are able to statistically explore how the force distribution and the force network anisotropy evolve with the shear stress.

Figure 3 shows the evolution of the force distribution with the shear stress at $\phi = 0.65$ and 0.70, averaged over 10000 states for each stress. At both volume fractions, there is a maximum in $P(F)$ at small F. However, the maximum is more pronounced and shifts to a higher value of $F/\langle F\rangle$ at $\phi = 0.70$ than that at $\phi = 0.65$, where $\langle F\rangle$ is the average contact force. Moreover, the large F tail of $P(F)$ at $\phi = 0.65$ is exponential, while it decays faster than exponential at $\phi = 0.70$, as previously reported.[27] The more remarkable difference between the two volume fractions is their distinct responses to the increase of the applied shear stress. At $\phi = 0.65$, when the shear stress approaches the yield stress, the maximum at small F is lowered and broadened, and $P(F)$ increases significantly at large F. This indicates that there are more large force contacts under a larger shear stress. However, at $\phi = 0.70$, $P(F)$ is almost constant under all the shear stresses, so the number of large force contacts does not change apparently, unlike at $\phi = 0.65$. The much stronger response of $P(F)$ to the applied shear stress at $\phi = 0.65$ than that at $\phi = 0.70$ evidences the growth of the susceptibility, if the susceptibility is defined as the response of $P(F)$ to the applied shear stress. The susceptibility is directly linked to the spatial correlation, assuming that the fluctuation-dissipation theorem is satisfied, so the spatial correlation is expected to grow approaching point J, implying again the criticality of point J. To verify this picture, more thorough and intensive future work is needed to quantify the volume fraction dependence of the susceptibility and find if it exhibits any critical scaling.

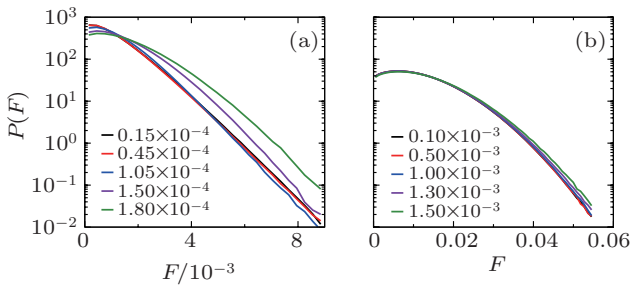


Fig. 3. Contact force distributions $P(F)$ of jammed solids consisting of $N = 1024$ particles at (a) $\phi = 0.65$ and (b) $\phi = 0.70$ with different shear stresses labeled in the legends.

As suggested by the previous studies,[31–33] the average contact force $\langle F\rangle$ separates the force network of a jammed solid into two subnetworks, a strong one ($F > \langle F\rangle$) and a weak one ($F < \langle F\rangle$). The strong network is load bearing and percolating, while the weak one is dissipative and does not support the load. When subject to a planar shear with the shear direction in the x direction and the shear gradient in the z direction, it is expected that the strong network consists of force chains aligned in the x–z plane to resist the shear. To verify this and to see how the force network anisotropy evolve with the shear stress, we show in Fig. 4 the distribution of the angle θ defined in the inset of Fig. 4(a). For each contact, we are concerned about two angles θ and β in the spherical coordinates, as illustrated in the inset of Fig. 4(a). In Fig. 4, we focus on the distribution of θ, $P(\theta)$, satisfying $\int_{0^\circ}^{180^\circ} P(\theta)\sin(\theta)\,\mathrm{d}\theta = 1$, for contacts lying in $\beta \in [135^\circ, 225^\circ]$ that are mostly affected by the shear.

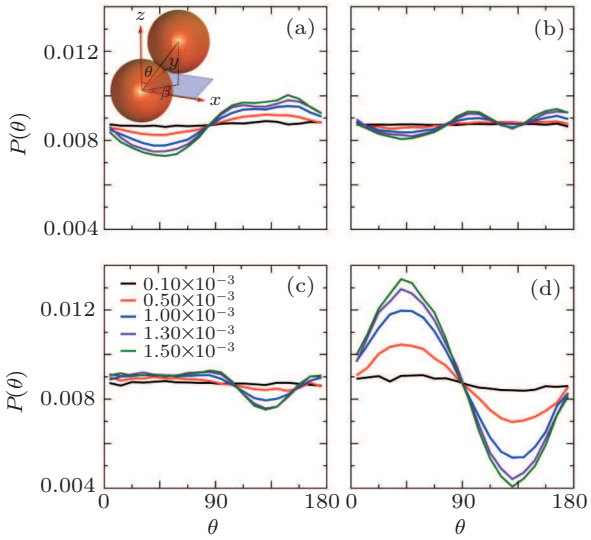


Fig. 4. Distribution of angle θ of particle contacts, $P(\theta)$, measured in four force windows ((a) [0, 0.005], (b) [0.005, 0.0115], (c) [0.0115, 0.015], and (d) [0.030, 0.040]) for jammed solids consisting of $N = 1024$ particles at $\phi = 0.70$. The average force is $\langle F\rangle = 0.0115$. The five curves in each panel are measured under different shear stresses, as shown in the legend. The inset illustrates the definitions of angles θ and β.

Near point J, the average force changes apparently with the shear stress, as shown in Fig. 3, so the self-averaging disappears.[27] Moreover, the fluctuations become larger approaching point J. Both effects lead to uncertainties in the quantification of the force network anisotropy. In Fig. 4, we demonstrate the evolution of the force network anisotropy at $\phi = 0.70$ because the force distribution is almost independent of the shear stress, we can then focus on the anisotropy without being disturbed by other changes.

We divide the whole force network into many subnetworks. In each subnetwork, the forces are within the same force window. In Fig. 4, we show the evolution of $P(\theta)$ with

the shear stress in four force windows. Panels (a) and (b) are below the average force $\langle F\rangle \approx 0.0115$, while panels (c) and (d) are above. Interestingly, $\langle F\rangle \approx 0.0115$ acts as a boardline. The general shape of $P(\theta)$ at $F > \langle F\rangle$ is symmetric to that at $F < \langle F\rangle$ with respect to $\theta = 90^\circ$. This validates the use of $\langle F\rangle$ to separate strong and weak contacts. For the weak subnetworks with $F \ll \langle F\rangle$, there is a minimum in $P(\theta)$ at $\theta \approx 45^\circ$, which decreases when increasing the shear stress, while the majority of the weak contacts point to a θ lying in $(90^\circ, 180^\circ)$. For the strong subnetworks with $F \gg \langle F\rangle$, the majority of the contacts point to $\theta \approx 45^\circ$, indicating that the strong contacts tend to form force chains perpendicular to the weak contacts. One may expect that the weak contacts mostly point to $\theta \approx 135^\circ$, which is approximately true, a peak in $P(\theta)$ appears at $\theta \approx 135^\circ$ when the forces are much smaller than $\langle F\rangle$ and the shear stress is small, as shown in Fig. 4(a). However, when F is close to $\langle F\rangle$ and the shear stress is large, the peak at $\theta = 135^\circ$ splits into two peaks at around 100° and 170°, as shown in Fig. 4(b). Such a split has not been observed before, which is more pronounced with the increase of the shear stress. When the forces are slightly larger than $\langle F\rangle$, as shown in Fig. 4(c), the effect of the split still exists and leads to an asymmetric $P(\theta)$, as well under large shear stresses. The occurrence of the split and its dependence on the shear stress are not trivial because it is robust near $\langle F\rangle$ and under large shear stresses, which deserves further investigation. When the forces are much larger than $\langle F\rangle$, figure 4(d) indicates that those forces are increasingly aligned in the principle direction at $\theta = 45^\circ$ when increasing the shear stress, which should be the main supporters of the shear.

6. Conclusions

Following Ref. [7], we study the mechanical properties of the jammed solids under a constant shear stress and compare the results from CS and QS samplings. All of our analyses are benefited from the CS sampling, which can unbiasedly explore the potential energy landscape under a constant shear stress and search for jammed solids under a desired shear stress. Although most of the analyses can be performed using the QS sampling, we have demonstrated that the QS sampling is biased and cannot accurately control the shear stress and is thus awkward in the study of the shear stress dependence.

For finite size systems, the QS sampling leads to a smaller yield stress and a larger average critical volume fraction of the jamming transition at point J ($T = 0$ and $\sigma = 0$). In the thermodynamic limit, our analysis suggests that the differences between the two samplings vanish. By statistically measuring the shear modulus as a function of the shear stress, we find that the shear modulus decreases with the increase of the shear stress. However, the shear modulus does not decay to zero at yielding, implying the discontinuous nature of the unjamming transition at $\sigma > 0$. The discontinuity is further verified by the discontinuous jump of the pressure at yielding from jammed solids to unjammed shear flows. The pressure jump decreases with decreasing shear stress and shows the trend to vanish at point J when $\sigma = 0$, which is analogous to the typical phase transitions under an external field. Moreover, we investigate the evolution of the force distribution and the force network anisotropy. The force distribution shows a weak shear stress dependence away from point J, while it is sensitive to the change of the shear stress near point J, again implying the criticality of point J. When subject to a shear stress, the strong contact forces are aligned in the direction of $\theta = 45^\circ$ to support the shear, while the weak forces distribute around $\theta = 135^\circ$. Interestingly, when the forces are close to the average force and the shear stress is large, the peak in the distribution $P(\theta)$ at $\theta = 135^\circ$ splits into two peaks, which leads to an asymmetric $P(\theta)$. The underlying physics of this split requires further investigation.

References

[1] Liu A J and Nagel S R 1998 *Nature* **396** 21
[2] O'Hern C S, Silbert L E, Liu A J and Nagel S R 2003 *Phys. Rev. E* **68** 011306
[3] Xu N 2011 *Front. Phys.* **6** 109
[4] van Hecke M 2010 *J. Phys.: Condens. Matter* **22** 033101
[5] Andrea J L and Nagel R 2010 *Annu. Rev. Condens. Matter. Phys.* **1** 347
[6] Ikeda A, Berthier L and Sollich P 2012 *Phys. Rev. Lett.* **109** 018301
[7] Liu H, Xie X and Xu N 2014 *Phys. Rev. Lett.* **112** 145502
[8] Vågverg D, Valdez-Balderas D, Moore M A, Olsson P and Teitel S 2011 *Phys. Rev. E* **83** 030303
[9] Chaudhuri P, Bethier L and Sastry S 2010 *Phys. Rev. Lett.* **104** 165701
[10] Silbert L E, Liu A J and Nagel S R 2005 *Phys. Rev. Lett.* **95** 098301
[11] Wyart M, Silbert L E, Nagel S R and Witten T A 2005 *Phys. Rev. E* **72** 051306
[12] Wyart M, Nagel S R and Witten T A 2005 *Europhys. Lett.* **72** 486
[13] Ellenbroek W G, Somfai E, van Hecke M and van Saarloos W 2006 *Phys. Rev. Lett.* **97** 258001
[14] Olsson P and Teitel S 2007 *Phys. Rev. Lett.* **99** 178001
[15] Hatano T 2008 *Phys. Soc. Jpn.* **77** 123002
[16] Drocco J A, Hastings M B, Reichhardt C J O and Reichhardt C 2005 *Phys. Rev. Lett.* **95** 088001
[17] Ozawa M, Kuroiwa T, Ikeda A and Miyazaki K 2012 *Phys. Rev. Lett.* **109** 205701
[18] Tighe B P, Woldhuis E, Remmers J J C, van Saarloos W and van Hecke M 2010 *Phys. Rev. Lett.* **105** 088303
[19] Durian D J 1995 *Phys. Rev. Lett.* **75** 4780
[20] Xu N, Vitelli V, Wyart M, Liu A J and Nagel S R 2009 *Phys. Rev. Lett.* **102** 038001
[21] Vitelli V, Xu N, Wyart M, Liu A J and Nagel S R 2010 *Phys. Rev. E* **81** 021301
[22] Zhao C, Tian K and Xu N 2011 *Phys. Rev. Lett.* **106** 125503
[23] Keys A S, Abate A R, Glotzer S C and Durian D J 2007 *Nat. Phys.* **3** 260
[24] Head D A 2009 *Phys. Rev. Lett.* **102** 138001
[25] Heussinger C and Barrat J L 2009 *Phys. Rev. Lett.* **102** 218303
[26] Jaeger H M, Nagel S R and Behringer R P 1996 *Rev. Mod. Phys.* **68** 1259
[27] O'Hern C S, Langer S A, Liu A J and Nagel S R 2002 *Phys. Rev. Lett.* **88** 075507

[28] Corwin E I, Jaeger H M and Nagel S R 2005 *Nature* **435** 1075
[29] Mueth D M, Jaeger H M and Nagel S R 1998 *Phys. Rev. E* **57** 3164
[30] Blair D L, Mueggenburg N W, Marshall A H, Jaeger H M and Nagel S R 2001 *Phys. Rev. E* **63** 041304
[31] Radjai F, Wolf D E, Jean M and Moreau J J 1998 *Phys. Rev. Lett.* **80** 61
[32] Majmudar T S and Behringer R P 2005 *Nature* **435** 1079
[33] Radjai F, Roux S and Moreau J J 1999 *Chaos* **9** 544
[34] Malandro D L and Lacks D J 1999 *J. Chem. Phys.* **110** 4593
[35] Maloney C E and Lemaître A L 2006 *Phys. Rev. E* **74** 016118
[36] Tanguy A, Leonforte F and Barrat J L 2006 *Eur. Phys. J. E* **20** 355
[37] Heussinger C, Chaudhuri P and Barrat J L 2010 *Soft Matter* **6** 3050
[38] Andreotti B, Barrat J L and Heussinger C 2012 *Phys. Rev. Lett.* **109** 105901
[39] Allen M P and Tildesley D J 1987 *Computer Simulation of Liquids* (Oxford: Clarendon Press)
[40] Bitzek E, Koskinen P, Gähler F, Moseler M and Gumbsch P 2006 *Phys. Rev. Lett.* **97** 170201
[41] Larson R G 1999 *The Structure and Rheology of Complex Fulids* (Oxford: Oxford University Press)
[42] Xu N and O'Hern C S 2006 *Phys. Rev. E* **73** 061303
[43] Coussot P, Nguyen Q D, Huynh H T and Bonn D 2002 *Phys. Rev. Lett.* **88** 175501